Nonlin. Processes Geophys. Discuss., 1, 583–613, 2014
www.nonlin-processes-geophys-discuss.net/1/583/2014/
doi:10.5194/npgd-1-583-2014

Nonlinear Processes in Geophysics
Discussions
Open Access

Conjugate fluctuation analysis for a set of 41 magnetic clouds measured by the ACE spacecraft

A. Ojeda González[1,3,4], W. D. Gonzalez[1], O. Mendes[1], M. O. Domingues[2], and R. R. Rosa[2]

[1]DGE/CEA/National Institute for Space Research – INPE 12227-010 São José dos Campos, SP, Brazil
[2]LAC/CTE/National Institute for Space Research – INPE 12227-010 São José dos Campos, SP, Brazil
[3]Department of Space Geophysics, Institute of Geophysics and Astronomy – IGA Havana City, Cuba
[4]Junior Postdoctoral Fellow – CNPq/Brasilia – DF, Brazil

Received: 24 February 2014 – Accepted: 19 March 2014 – Published: 11 April 2014

Correspondence to: A. Ojeda González (ojeda.gonzalez.a@gmail.com)

Published by Copernicus Publications on behalf of the European Geosciences Union & American Geophysical Union.

Abstract

The statistical distribution of values in the signal and the autocorrelations (interpreted as the memory or persistence) between values are attributes of a time series. The autocorrelation function values are positive in a time series with persistence, while it are negative in a time series with anti persistence. The persistence of values with respect to each other can be strong, weak, or nonexistent. A strong correlation implies a "memory" of previous values in the time series. The long-range persistence in time series could be studied using semivariograms, rescaled-range, detrended fluctuation analysis and Fourier spectral analysis, respectively. In this work the persistence analysis has been used to study IMF time series. We use data from the IMF GSM-components with time resolution of 16 s. Time intervals corresponding to distinct processes around 41 MCs in the period between March 1998 and December 2003 were selected. In this exploratory study the purpose with this selection is to deal with the cases presenting the three periods: plasma sheath, MC and post-MC. We calculated one exponent of persistence (e.g., α, β, *Hu*, *Ha*) over the previous three time intervals. The persistence exponent values increased inside cloud regions, and it was possible select the following threshold values: $\langle \alpha_{(j)} \rangle = 1.392$; $\langle Ha_{(j)} \rangle = 0.327$; $\langle Hu_{(j)} \rangle = 0.875$. These values are useful as another test to evaluate the quality of the identification. If the cloud is well-structured, then the persistence exponents values exceed thresholds. In 80.5 % of the cases studied, these tools were able to separate the region of the cloud from neighboring regions. The Hausdorff exponent (*Ha*) provides the best results.

1 Introduction

Coronal Mass Ejection (CMEs) are massive expulsions of magnetized plasma from the solar atmosphere (Dasso et al., 2005). As a consequence of this ejection, CMEs can form confined magnetic structures with both extremes of the magnetic field lines connected to the solar surface, extending far away from the Sun into the solar wind (SW). Solar Ejecta (also known as Interplanetary Coronal Mass Ejections, ICMEs)

NPGD
1, 583–613, 2014

are the interplanetary manifestation of CMEs events (Dasso et al., 2005). The important subset of ICMEs known as interplanetary magnetic clouds (MCs), a term introduced by Burlaga et al. (1981), is characterized fundamentally by enhanced magnetic field strengths with respect to solar wind ambient values (Klein and Burlaga, 1982; Burlaga, 1991). A cloud ejected from the Sun can be simulated using a toroidal geometry. Its evolution and propagation through the solar wind can be studied using three-dimensional magnetohydrodynamic self-consistent numerical simulations (Vandas et al., 2002). A comprehensive study about the properties of MCs at 1 astronomical unit (AU) was approached by Ojeda et al. (2013), Ojeda et al. (2014), and Klausner et al. (2014).

The test for independence and searching for correlations in a time series can be carried out by use of an analytical tool from nonlinear dynamics, the estimation of the Hurst exponent (Hurst et al., 1965). It was first used by Mandelbrot and Wallis (1969) to study a series of monthly sunspot of 200 years. It had a Hurst exponent (with rescaled range – R / S) significantly larger than 0.5. On others papers such as Ruzmaikin et al. (1994), they showed that the solar activity have long-term persistence when explore time series of ^{14}C (Carbone-14). Calzadilla and Lazo (2001); Wei et al. (2004) studied time series of D_{st} geomagnetic index which showed chaotic properties in association with self-affine fractals. The D_{st} index can be viewed as a self-affine fractal dynamic process, as result of SW–magnetosphere interactions. In fact, the behavior of the D_{st} index, with a Hurst exponent $Hu \approx 0.5$ (power-law exponent $\beta \approx 2$) at high frequency, is similar to that of Brownian motion. Therefore, perhaps the dynamical invariants of some physical parameters of the solar wind, specifically the MCs, may have spectral characteristics similar to Brownian motion.

Price and Newman (2001) analyzed the behavior of solar wind dataset (IMF and solar wind speed) with 1 min resolution from September 1978 to July 1979 using the ISEE-3 spacecraft. They showed the time series, the power spectrum and the R / S analysis for the IMF B_z component for the month of March 1979. The B_z time series was self-similar for all time scales, highly coherent for time scales less than one day,

NPGD
1, 583–613, 2014

and only slightly coherent for time scales greater than one day. Also, they found self-similarity and coherence properties when calculated β-power spectrum values to vB_z, AE index and the horizontal (H) component of the Earth's magnetic field.

In this paper, a detailed study of persistence in magnetic clouds has been realized. The manuscript has been divided in five sections. A review about persistence analysis is presented in the Sect. 2. In Sect. 3 presents the dataset and the analyzed periods. In Sect. 4 presents the methodology implemented. In Sect. 5, the results are discussed. We have interested in using the persistence exponents to characterize MCs. In Sect. 6, the conclusions are shown.

2 Persistence in time series

In this work the persistence analysis has been used to study IMF time series. The purpose throughout this section is to review the physical-mathematical concepts of these tools.

The main attributes of a time series include the statistical distribution of values in the signal and the autocorrelations (interpreted as the memory or persistence) between values. Positive values of autocorrelation function, $r_k = C_k/C_0$, indicate persistence while negative value indicate antipersistence. For example, in a Gaussian white noise each time series value is independent of other values, then the correlation and the persistence are zero. Time series of Brownian motion is derived from a running sum of a Gaussian white-noise sequence. The values in a time series of a Brownian motion are well-correlated, then this time series exhibits long-range persistence. In summary, the persistence can be grouped in three categories: strong, weak, or nonexistent.

The word "memory" is the common term to explain and understand persistence concept in a time series. The values in the time series could be considered "intelligent entities" that have "knowledge" or "memory" of the existence of other "individuals" (values). The ideal case of maximum persistence is when each value has memory of the all previous values of the time series. Thus, a strong correlation implies a "memory" of

NPGD
1, 583–613, 2014

previous values in the time series. Persistence is a mathematical number to measure how good is the "mean memory" in a time series. The long-range persistence in time series could be studied using semivariograms, rescaled-range, detrended fluctuation analysis, Fourier spectral analysis, and wavelet variance analysis respectively (e.g., Malamud and Turcotte, 1999).

A statistically self-similar fractal can be define with the function $f(rx, ry)$ (with scaling factor r) in two-dimensional xy space. This fractal is by definition isotropic and the previous function is statistically similar to $f(x, y)$ and it is quantified by the fractal relation $N_i \sim r_i^{-D}$ where the number of objects, N_i, and the characteristic linear dimension, r_i, are related by a power law, and the constant exponent, D, is the fractal dimension (Turcotte, 1997).

A statistically self-affine fractal can be define with the function $f(rx, r^{Ha}y)$ (generally not isotropic) in two-dimensional xy space, where Ha is called Hausdorff exponent. The previous function is statistically similar to $f(x, y)$ (Mandelbrot, 1983; Voss, 1985b) and the relationship between Ha and D is $Ha = 2 - D$ (e.g., Malamud and Turcotte, 1999). If $Ha = 1$ then the self-affine fractal is at the same time self-similar. Brownian motion is a example of self-affine time series.

The power spectrum of a time series is the Fourier transform of the autocorrelation function. The power spectrum (Priestley, 1981), a measure of long-range persistence and antipersistence, is used frequently in the analysis of geophysical time series (e.g., Pelletier and Turcotte, 1999). The periodogram is a plot of power-spectral density (PSD) of a signal $S(f)$ vs. frequency f, it is an estimate of the spectral density of a signal. For a time series that is self-affine, $S(f) \sim f^{-\beta}$ (e.g., Voss, 1985a) where the slope of the best-fit straight line from $\log(S(f))$ vs. $\log(f)$ is a constant called β-power spectrum exponent. The relationship between β, Ha, and D was obtained by Voss (1986):

$$\beta = 2Ha + 1 = 5 - 2D \quad (1)$$

In the paper of Malamud and Turcotte (1999), validation intervals for a self-affine fractal were derived: $0 \leq Ha \leq 1$, $1 \leq D \leq 2$, and $1 \leq \beta \leq 3$. Then, in a time series of a Brown-

NPGD
1, 583–613, 2014

ian motion the exponent values are $Ha = 1/2$, $D = 3/2$, $\beta = 2$ while a white noise has $\beta = 0$. Hausdorff exponent is only applicable for self-affine time series with validation intervals from $0 \leq Ha \leq 1$, however β is a measure of the strength of persistence valid for all β, not just $1 \leq \beta \leq 3$ (Malamud and Turcotte, 1999). An antipersistent time series has $\beta < 0$ and persistent time series has $\beta > 0$, respectively.

Mandelbrot and Ness (1968) developed a method to study a self-affine time series, the semivariogram, γ_k, scale with k, the lag, such that $\gamma_k \sim k^{2Ha}$, that is:

$$\gamma_k = 2^{-1}(N-k)\sum_{n=1}^{N-k}(y_{n+k}-y_n)^2. \quad (2)$$

For the uncorrelated Gaussian white noise ($\beta = 0$), the semivariogram is about $\gamma_k = 1$, the same as the variance, $V_a = 1$. For $\beta = 1$, 2 and 3, good correlations are obtained by Malamud and Turcotte (1999, p. 40) with the expression $\gamma_k \sim k^{2Ha}$.

Following Malamud and Turcotte (1999) is possible read, that other alternative method to measure the persistence in time series was developed by Hurst (1951); Hurst et al. (1965). They studied the Nile River flow as a time series to introduce the concept of rescaled-range (R / S) method used to calculate the scaling exponent (Hurst exponent), *Hu*, to give quantitative measure of the persistence of a signal. Hurst (1951); Hurst et al. (1965) found empirically the power–law relation:

$$\left[\frac{R(\tau)}{S(\tau)}\right]_{\text{av}} = \left(\frac{\tau}{2}\right)^{Hu} \quad (3)$$

where the successive subintervals τ varies over all N values in the time series, y_n. The running sum, y_m, is:

$$y_m = \sum_{n=1}^{m}(y_n - \overline{y}_N). \quad (4)$$

NPGD
1, 583–613, 2014

The range is defined by $R_N = (y_m)_{\max} - (y_m)_{\min}$ with $S_N = \sigma_N$ where $\overline{y}_N$ and σ_N are the mean and standard deviation of all N values in the time series, y_n. The R / S analysis is a statistical method to analyse long records of natural phenomena (Vanouplines, 1995).

Tapiero and Vallois (1996) found that $0.5 < Hu \leq 1.0$ implies persistence and that $0 \leq Hu < 0.5$ implies antipersistence. This would imply that (Tapiero and Vallois, 1996; Malamud and Turcotte, 1999):

$$\beta = 2Hu - 1 = 2Ha + 1 \tag{5}$$

The Eq. (5) only has a small validation region (see Malamud and Turcotte, 1999, Figs. 17 and 25). This result should be considered when an exponent is derived from another.

Other technique (called detrended fluctuation analysis (DFA)) to study persistence in time series was introduced by Peng et al. (1994). Also this tool could be used to study persistence on IMF time series.

The fluctuation function $F(L)$ is construct over the whole signal at a range of different window size L where $F(L) \sim L^{\alpha}$. The obtained exponent, α, is similar to the Hurst exponent, but it also may be applied to non-stationary signals, this is a great advantage. DFA measures scaling exponents from non-stationary time series for determining the statistical self-affinity of an underlying dynamical non-linear process (e.g., Veronese et al., 2011). It is useful for characterizing temporal patterns that appear to be due to long-range memory stochastic processes (Veronese et al., 2011). A detailed description of this method, step by step, see Peng et al. (1994), Baroni et al. (2010), Veronese et al. (2011), and Little et al. (2006).

Based on the Wiener–Khinchin theorem (Kay and Marple, 1981), it is possible to show that the two exponents β (from PSD) and α (from DFA) are related by:

$$\beta = 2\alpha - 1. \tag{6}$$

NPGD
1, 583–613, 2014

For fractional Brownian motion we have $1 \leq \beta \leq 3$, and then $1 \leq \alpha \leq 2$. The exponent of the fluctuations can be classified according to a dynamic range values (Kantelhardt et al., 2002; Bashan et al., 2008; Zheng et al., 2008):

- $\alpha < \frac{1}{2}$: anti-correlated, antipersistence signal.
- $\alpha \cong \frac{1}{2}$: uncorrelated, white noise, no memory.
- $\alpha > \frac{1}{2}$: long-range persistence.
- $\alpha \cong 1$: $1/f$ noise or pink noise.
- $\alpha > 1$: non-stationary, random walk like, unbounded.
- $\alpha \cong \frac{3}{2}$: Brownian noise or red noise.

Polynomial of different order could be used during the computacional implementation of the DFA method. For example, DFAn uses polynomial fits of order n (Buldyrev et al., 1995). DFA1 (used in this work) only removes constant trends in the time series, and it is equivalent to Hurst R / S analysis. Effect of trends on DFA were studied in Hu et al. (2001) and the relation to the power spectrum method is presented in Heneghan and McDarby (2000). Veronese et al. (2011) showed that DFA method is especially useful for short records of stochastic and non-linear processes.

The four techniques explained previously are used in this work. As some models were tested with success to reconstruct the magnetic structure of MCs (Dasso et al., 2005; Ojeda et al., 2013), this imply that exist a memory in the time series of IMF. We have the hypothesis that magnetic field inside of these structures has bigger persistence than ambient solar wind. If the previous hypothesis is true, then the persistence exponent could be transform in an auxiliary tool to study MCs. We decided to test the four techniques because only has a small validation region between them (see Malamud and Turcotte, 1999, Figs. 17 and 25). The ideal is to use as many as possible techniques to measure the persistence, and to compare between them.

NPGD
1, 583–613, 2014

3 IMF dataset

In this work we use data from the IMF GSM-components (ACE spacecraft/MAG instrument) with time resolution of 16 s. We work with 41 of 80 events (73 MCs and 7 cloud candidate) identified by Huttunen et al. (2005). These events in chronological order are shown in Table 1 (see more details in Ojeda et al., 2013, 2014, where the same dataset was studied with other techniques: the spatio-temporal entropy and discrete wavelet transform). The columns from the left to the right give: a numeration of the events, year, shock time (UT), MC start time (UT), MC end time (UT), and the end time (UT) of the third region respectively. In this exploratory study the purpose with this selection is to deal with the cases presenting the three periods (clear Pre-MC or Plasma Sheath, MC and Post-MC).

4 Methodology

To calculate the persistence exponents were used the following computational programs:

1. If we installed GNU/Octave then a hurst(x) function is created for example in /usr/share/octave/3.0.1/m/signal/. The function is used to calculate the Hurst exponent (Hu).
2. Following the work of Malamud and Turcotte (1999), we did a program in GNU/Octave to calculate the Hausdorff exponent (see Appendix A).
3. A program using GNU/Octave was implemented by McSharry and Malamud (2010) to calculate the β exponent.
4. A fast Matlab implementation[1] of the DFA algorithm was performed by Little et al. (2006).

[1] http://www.maxlittle.net/software/.

NPGD
1, 583–613, 2014

The behavior of the persistence in time series of the IMF components, measured by the ACE spacecraft with a time resolution of 16 s is explored. We studied the persistence between time series corresponding to sheaths, MCs and a quiet SW after the MC (post-MC) with equivalent time duration to it. We calculate one exponent of persistence (e.g., α, β, Hu, Ha) over each of three time intervals corresponding to distinct processes. For example, persistence in the case numbered as 1 in Table 1 is studied. The interval from 6 January 13:19 UT to 7 January 02:59 UT was classified as the sheath region. In the sheath the persistence exponents to B_x component are calculated. These values are: $\alpha = 1.27$, $\beta = 1.71$, $Hu = 0.86$, $Ha = 0.31$, respectively.

The interval from 7 January 03:00 UT to 8 January 09:00 UT is the MC region. The post-MC region was selected from 8 January 09:01 UT to 9 January 15:00 UT. The persistence exponents are shown in Table 2 rows 4 and 5 respectively.

The previous methodology is extended for the others two components, i.e., B_y and B_z respectively. In Table 2 rows 6–13 the results are shown.

MCs exhibit flux-rope characteristics: a large-scale winding of a closed magnetic structure that is nearly force-free. And it is possible to see anisotropy of magnetic field fluctuations in an average interplanetary MC at 1 AU (Narock and Lepping, 2007; Ojeda et al., 2013, 2014). We do not expect to find the same behavior in all three components by the existence of anisotropy. The anisotropic behavior, in our opinion, is caused by the geometry of flux-rope and the axis inclination angle. We have interest in a single value to characterize the persistence in the IMF, for this reason a mean persistence value using the three IMF components is calculated at each time. It is the only form that we found to quantify the persistence in all structure and to minimize the anisotropy in the calculation. The mathematical expressions can be generalized in the following

NPGD
1, 583–613, 2014

equations:

$$\langle \beta_{(j)} \rangle = \frac{1}{3} \sum_{i=1}^{3} \beta_{(j)}^{(i)}. \tag{7}$$

$$\langle \alpha_{(j)} \rangle = \frac{1}{3} \sum_{i=1}^{3} \alpha_{(j)}^{(i)}. \tag{8}$$

$$\langle Hu_{(j)} \rangle = \frac{1}{3} \sum_{i=1}^{3} Hu_{(j)}^{(i)}. \tag{9}$$

$$\langle Ha_{(j)} \rangle = \frac{1}{3} \sum_{i=1}^{3} Ha_{(j)}^{(i)}. \tag{10}$$

The angle brackets $\langle \cdots \rangle$ denote an average of the IMF components ($i = 1,2,3 = B_x, B_y, B_z$), also the standard deviation is calculated. Each of the three regions are represented in one j value: $j = 1 \equiv$ sheath, $j = 2 \equiv$ MC, $j = 3 \equiv$ post-MC.

In Table 2, the average and standard deviation values for all persistence exponents are shown. In Table 2, as we thought, the persistence values increases inside the MC. This increase, according to the hypothesis raised in the end of Sect. 2, was expected. The previous idea is not always true when using the spectral-power β exponent. However, one of the main problems in using a discrete Fourier transform are spectral variance and leakage (Priestley, 1981; Percival and Walden, 1993). This show a range of uncertainty in the values of β. The other problem is the nonstationarity of the IMF components. The previous study was generalized for a group of 41 events shown in Table 1; and will be discussed in next section.

NPGD
1, 583–613, 2014

5 Results and discussion

Initially, the persistence analysis is done to establish a preliminary categorization of the periods in the SW related to the MC occurrences.

5.1 Persistence analysis on the IMF variation

The methodology that uses the persistence exponents (see Sect. 4) is applied to 41 events. Using Eq. (7) the $\langle\beta_{(j)}\rangle$ values are calculated. The $\langle\beta_{(j)}\rangle$ values for the 41 events (Sheath, MC, and post-MC) are shown in Fig. 1a. The three intervals of time for each event were plotted as "□", "⊗", and "Δ" symbols respectively. The error bar represents the standard deviation for each value. It is shows the power spectral density (PSD) scaling exponent $\langle\beta_{(j)}\rangle$ as a self-affine fractal ($1 < \langle\beta_{(j)}\rangle < 2$) but there is not a pattern that allows the separation of MC from the other two cases; exist a total of 18/41 events where the clouds do not have the larger values. We understand that in non-stationary time series the Fourier transform is not suitable, because the core functions of the transform is composed of sines and cosines.

For short time series, DFA can detect the correlation length more accurately than the PSD scaling exponent (β) (Veronese et al., 2011). The alpha exponent value is not affected by spectral variance and leakage and is possible to use in non-stationary time series. Figure 1b has the same format that Fig. 1a, but was built for $\langle\alpha_{(j)}\rangle$ exponent using the Eq. (8). The results show $\langle\alpha_{(j)}\rangle$ values from 1.00 to 1.60, i.e., long-range persistence and some MCs with typical values of a Brownian noise ($\langle\alpha_{(j)}\rangle \cong 1.50$).

In 38 of the 41 events, the alpha ($\langle\alpha_{(j)}\rangle$) value in the MC ("⊗") is larger than the one in the sheath ("□") respectively. We seen some exceptions, the events 5, 20, and 25 that shown in Table 1. We did not stop to examine these cases in detail, it are few for the statistics of 41 cases. Nevertheless, it is recommended to study in the future, because we think that could be need to redefine the cloud boundaries.

Also, the Hurst exponent was presented in Sect. 4 as an useful methodology to study MCs. Using the Eq. (9), the $\langle Hu_{(j)}\rangle$ exponents in the three regions are calculated. Fig-

NPGD
1, 583–613, 2014

ure 1c has the same format that Fig. 1a and b respectively, but for $\langle Hu_{(j)} \rangle$ exponent. Similar to Fig. 1b, the $\langle Hu_{(j)} \rangle$ exponents have larger values in the MC. Nevertheless, 4/41 MC (events 11, 19, 28, and 30) does not have largest $\langle Hu_{(j)} \rangle$ exponents in MC region. None of this cases coincide with the three events (5, 20, and 25) when the alpha exponent is used. This draws attention to have a certain degree of distrust in the identification of these clouds, but also suggest that all techniques must be used together to increase the confidence level in the results. Still in 34/41 events both exponents have largest values in the cloud region.

The last tool to use is the Hausdorff exponent (*Ha*). To calculate the mean Hausdorff exponents, the Eq. (10) is used. In Fig. 1d, the $\langle Ha_{(j)} \rangle$ exponents have largest values in the MC regions, only 2/41 MC (events 10 and 28) does not have largest $\langle Ha_{(j)} \rangle$ exponents. Thus, this tool provides the best results.

In conclusion, the PSD scaling exponent is not a suitable tool to study persistence in IMF components in the SW. The three exponents report the largest persistence in 33 of total 41 MC regions. In 80.5 % from 41 cases, these tools were able to separate the region of the cloud of neighboring regions.

To make a comparison between all events, it is necessary to build a histogram. In Fig. 2a, the histogram was built from a frequency table of $\langle \beta_{(j)} \rangle$ values plotted in Fig. 1a. The $\langle \beta_{(j)} \rangle$ values for the sheath, MC and post-MC regions where plotted as gray, black and white bar respectively. The bars have an uniform distribution from $1.5 < \langle \beta_{(j)} \rangle < 1.8$. For $\langle \beta_{(j)} \rangle < 1.5$, there are 7/41 sheath, 2/41 MC and 15/41 post-MC events, while for $\langle \beta_{(j)} \rangle > 1.8$ there are 3/41 sheath, 9/41 MC and 3/41 post-MC events respectively. In previous comments was said that $\langle \beta_{(j)} \rangle$ exponent is not suitable to measure the persistence in the dataset used in this work. But even so, the largest values of $\langle \beta_{(j)} \rangle$ were found in the MCs.

Figure 2b has the same format that Fig. 2a, but for $\langle \alpha_{(j)} \rangle$ exponent. For $\langle \alpha_{(j)} \rangle > 1.4$, we have 6/41 sheath, 29/41 MC and 3/41 post-MC events respectively. So, we have many MCs with the largest alpha values. For $1.0 < \langle \alpha_{(j)} \rangle < 1.3$ the number of events by regions are 21/41 in the sheath, 3/41 in the MC and 23/41 in the post-MC. In MC

NPGD
1, 583–613, 2014

events, the separation of the $\langle \alpha_{(j)} \rangle$ values to the right corner is an interesting result. In the Fig. 2c and d, approximately 30/41 MC events have the largest values of the persistence exponents. One difficulty to study the persistence is the time series extension (Veronese et al., 2011). In Fig. 3, the histogram show the number of cases vs. temporal extension (in hour) of MCs and plasma sheaths respectively. The clouds extension is largest in the plasma sheaths. However, there are a pattern in the persistence values between all MC events. We believe that these results are valid, because we know that MCs are organized structures in the plasma (Ojeda et al., 2005, 2013, 2014) which have an increase of "memory" in the time series.

We considered a better way to view these results. Thus, the average values for each exponent from 41 events and for each of the three regions are calculated. The equations for calculating the average values are:

$$\langle \beta_{(j)} \rangle_T = \frac{1}{N} \sum_{i=1}^{N} \langle \beta_{(j)} \rangle^{(i)} \tag{11}$$

$$\langle \alpha_{(j)} \rangle_T = \frac{1}{N} \sum_{i=1}^{N} \langle \alpha_{(j)} \rangle^{(i)} \tag{12}$$

$$\langle Hu_{(j)} \rangle_T = \frac{1}{N} \sum_{i=1}^{N} \langle Hu_{(j)} \rangle^{(i)} \tag{13}$$

$$\langle Ha_{(j)} \rangle_T = \frac{1}{N} \sum_{i=1}^{N} \langle Ha_{(j)} \rangle^{(i)}, \tag{14}$$

with $N = 41$ and $j = 1 \equiv$ sheath, $j = 2 \equiv$ MC, $j = 3 \equiv$ post-MC.

The calculation of the standard deviation shows, how much variation or dispersion exists from the average. If a rectangular area was built using the mean and standard deviation then there are a validity region where join up all exponents. Following the above idea, the panels of Fig. 4 were built. In Fig. 4a the black points are $(\langle \alpha_{(j)} \rangle_T, \langle \beta_{(j)} \rangle_T)$

NPGD
1, 583–613, 2014

in each one of three regions, from 41 events plotted in the Fig. 1a and b. For 2-D graphic, filling is done in the x and y directions between the standard deviation of the mean, and the shade rectangular regions are the set of validations of the persistence for each regions. Thus, the graph allows a conjugate analysis of persistence. In Fig. 4a, we see in $\langle\beta_{(j)}\rangle_T$ axis that the MC is the region with the largest average value. But, shade rectangular regions are overlapping. It is not possible to separate the MC region. Still, the result is important because we can see that persistence is large in the MCs. On the other hand, if we see the $\langle\alpha_{(j)}\rangle_T$ axis then 75 % of the shade rectangular regions are not overlapping. The MCs have $\langle\alpha_{(j)}\rangle$ values from 1.390 to 1.540. A vertical dashed line is drawn in the point 1.392. We propose the use of this value as a threshold when the alpha exponent is calculated in a MC regions. Also, this values could be useful to create an identification methodology of MCs.

Figure 4b has the same format that Fig. 4a but in the y axis, $\langle Ha_{(j)}\rangle_T$ was plotted. Along $\langle Ha_{(j)}\rangle_T$ axis, the shaded rectangular region corresponding to the MC is less overlap with other regions than are seen in the previous Fig. 4a. Only the MCs have $\langle Ha_{(j)}\rangle$ values between 0.320 and 0.420. An horizontal dashed line is drawn in the point 0.327.

Figure 4c has the same format that Fig. 4a and b but in the y axis, $\langle Hu_{(j)}\rangle_T$ was plotted. Also the MCs were separated of the other two regions. And the horizontal dashed line is drawn in the point 0.875. The regions with least overlap correspond to the Hurst and Hausdorff exponents respectively. In Fig. 4d ($\langle Hu_{(j)}\rangle_T \pm\sigma$) vs. ($\langle Ha_{(j)}\rangle_T \pm\sigma$) is plotted. The Hurst and Hausdorff exponents provide good results and the clouds are separated from the other two regions. This graphic could be used to evaluate the quality when a new MC is identified using other methods, i.e., they are useful to categorize the ranges previously identified by other method.

With these results, we conclude that the persistence values increases in the IMF components inside of MCs. In this study the investigated period covers the rising phase of solar activity (1998–1999), solar maximum (2000) and the early declining phase (2001–2003) when defined by the yearly sunspot number. We have a variety of MCs

NPGD
1, 583–613, 2014

in five year (1998–2003) and the rotation of the magnetic field direction can occur in any direction relative to the ecliptic. But there are some MCs where identification is not completely secure. For example, WIND MC table[2] shown a quality factor (1 = Excellent, 2 = Good, 3 = Poor) when MC intervals are identified. This methodology can help to evaluate the quality of the identification. After identifying a MC, if their persistence exponents occupy non overlapping regions in Fig. 4 (panels b, c and d) then the cloud was identified with good quality. An advantage of the proposed methodology is that plasma data are not indeed required. The plasma data sometimes have large gaps and poor time resolution if compare with the magnetic field data.

6 Conclusions

The physical bases for the use of the techniques are the plasma features related to the MC processes. Physical-mathematical techniques have been selected for their skills in order to allow the investigation on MC occurrences. Those techniques have been developed in an original approach to characterize MC events in the SW. They consist in techniques of persistence exponents: Hurst, Hausdorff, beta exponent from power-spectral density (Fourier) and alpha exponent from detrended fluctuation analysis respectively. Those numerical tools have a great advantage because they are easy to implement with low computational cost and could allow creating an automatic operation detection. Also, they characterize MC regions using as input data only the three components of the interplanetary magnetic field (IMF) measured by satellites at convenient space location, e.g., the Lagrangian point $L1$.

We worked mainly with data of B_x, B_y, and B_z with temporal resolution of 16 s measured by the ACE. We worked with a total of 41 MCs from the years 1998–2003, published in the paper of Huttunen et al. (2005). The criteria used to select these 41 cases was the existence of a plasma sheath in front of the MC, and in these cases clouds

[2]http://wind.nasa.gov/mfi/mag_cloud_pub1.html.

NPGD
1, 583–613, 2014

were well-identified. We have studied persistence in the 41 ICMEs divided in three regions: plasma sheath, MC and post-MC respectively. The persistence exponent values increased inside cloud regions, and it was possible select the following threshold values: $\langle \alpha_{(j)} \rangle = 1.392$; $\langle Ha_{(j)} \rangle = 0.327$; $\langle Hu_{(j)} \rangle = 0.875$. These values are useful as another test to evaluate the quality of the identification. After identifying a cloud, the persistence analysis can be performed in the full extent of temporal series of the three IMF components. If the cloud is well-structured, then the persistence exponents values exceed thresholds.

The PSD scaling exponent is not a suitable tool to study persistence in IMF components in the SW. Nevertheless, the other three exponents are suitable to study persistence, and the exponents values have an increased in the cloud region. It means that the three exponents report the largest persistence in 33 of total 41 cloud regions. In 80.5 % of the cases studied, these tools were able to separate the region of the cloud from neighboring regions. The Hausdorff exponent (*Ha*) provides the best results.

One difficulty to study the persistence in time series is the dimension of it. However, we can see a pattern in the persistence values between all MC events. An additional analysis by other techniques that consider processes with non-Gaussian features and multifractality is underway and will be presented later (Campos-Velho et al., 2001; Bolzan, M. J. A. et al., 2002).

Appendix A

Autocorrelations and semivariograms

A summary taken from Malamud and Turcotte (1999) is presented here. The correlation of a time series with itself, i.e. $y(t+s)$ compare with $y(t)$ at lag s, is called autocorrelation function ($r(s)$). The autocorrelation function can be used to quantify the persistence or

NPGD
1, 583–613, 2014

antipersistence of a time series. This is given by:

$$r(s) = \frac{c(s)}{c(0)}, \tag{A1}$$

with the autocovariance function, $c(s)$, given by

$$c(s) = \frac{1}{(T' - s)} \int_0^{T'-s} [y(t+s) - \bar{y}][y(t) - \bar{y}]\,\mathrm{d}t,$$

and the autocovariance function at 0 lag, $c(0)$, given by

$$c(0) = \frac{1}{T'} \int_0^{T'} [y(t) - \bar{y}]^2\,\mathrm{d}t = V_a$$

The time series, $y(t)$, is prescribed over the interval $0 \le t \le T'$. The average and variance of $y(t)$ over the interval T' are $\bar{y}$ and V_a. The autocorrelation function, $r(s)$, is dimensionless and does not depend on the units of $y(t)$ or t. The plot of $r(s)$ vs. s is known as correlogram (Malamud and Turcotte, 1999).

For a discrete time series, the autocorrelation function, r_k, is given by:

$$r_k = \frac{c_k}{c_0} \tag{A2}$$

with the autocovariance, c_k, given by:

$$c_k = \frac{1}{(N-k)} \sum_{n=1}^{N-k} (y_{n+k} - \bar{y})(y_n - \bar{y}) \tag{A3}$$

NPGD
1, 583–613, 2014

and the autocovariance at 0 lag (the variance) given by:

$$c_0 = \frac{1}{N}\sum_{n=1}^{N}(y_n - \bar{y})^2 = V_a. \tag{A4}$$

If the mean or variance vary with the length of the interval considered, then the time series is nonstationary. The correlograms is inappropriate to study non stationary time series, because $r(s)$ has $\bar{y}$ in its definition. However, exist a method to measure long-range correlation which is valid for both stationary and nonstationary time series an alternative way, is the semivariogram γ. Like the autocorrelation function, the semivariogram measures the dependence of values in a time series that are separated by a lag, s.

For a discrete time series, the semivariogram, $\gamma(s)$, is given by:

$$\gamma_k = \frac{1}{2}(N-k)\sum_{n=1}^{N-k}(y_{n+k} - y_n)^2 \tag{A5}$$

For a stationary time series, the semivariogram, γ_k, and the autocorrelation function, r_k, are related. The mean of the time series, $\bar{y}$, can be added and subtracted within the summation in Eq. (A5) to give:

$$\gamma_k = \frac{1}{2(N-k)}\sum_{n=1}^{N-k}\left[(y_{n+k} - \bar{y}) - (y_n - \bar{y})\right]^2.$$

When expanded this gives:

$$\gamma_k = \frac{1}{2(N-k)}\left[\sum_{n=1}^{N-k}(y_{n+k} - \bar{y})^2 + \sum_{n=1}^{N-k}(y_n - \bar{y})^2 - \sum_{n=1}^{N-k}2(y_{n+k} - \bar{y})(y_n - \bar{y})\right]. \tag{A6}$$

NPGD
1, 583–613, 2014

Provided the time series is stationary, two of the terms in Eq. (A6) are equivalent to the variance in Eq. (A4), giving:

$$\gamma_k = V_a - \frac{1}{(N-k)} \sum_{n=1}^{N-k} (y_{n+k} - \bar{y})(y_n - \bar{y}). \quad \text{(A7)}$$

Substituting the definition for c_k from Eq. (A3) into Eq. (A7) and using the definitions of c_0 from Eq. (A4) and r_k from Eq. (A2), the new equation is:

$$\gamma_k = (V_a - c_k) = \left(V - V\frac{c_k}{c_0}\right) = V(1 - r_k) \quad \text{(A8)}$$

For an uncorrelated time series we have $r_k = 0$ and $\gamma_k = V_a$. Both the autocorrelation function and semivariograms have been applied by a number of author to both real and synthetic time series that exhibit long-range persistence (e.g. Ramos et al., 2004; Rosa et al., 2008).

Using the definition for the semivariogram, γ_k, given in Eq. (A5), a computational code was implemented:

```
function [Ha,R1] = Semivariogram(y)
N1 = size(y,1);
potencia2 = floor(log2(N1));
gammaT_k = 1 : potencia2;
xi = 1 : potencia2;
for i = 1 : potencia2
k = 2^i;
contador = 0;
for n = 1 : (N1 - k)
contador = contador + (y(n + k) - y(n))^2;
end
gam_k = (1/(N1 - k)) * contador;
```


NPGD
1, 583–613, 2014

```
gammaT_k(i) = gam_k;
xi(i) = k;
end
yi = gammaT_k;
[a,R] = RegresionLinear(log10(xi),log10(yi));
Ha = a/2;
R1 = R;
end
  function [a,R] = RegresionLinear(xi,yi)
n1 = size(xi,2);
a = (n1*sum(xi.*yi) - sum(xi)*sum(yi))/(n1*sum(xi.^2) - sum(xi)^2);
b = (sum(yi) - a*sum(xi))/n1;
R = ((sum(xi.*yi) - (sum(xi)*sum(yi))/n1)^2)/((sum(xi.^2) - (sum(xi)^2)/n1)*
(sum(yi.^2) - (sum(yi)^2)/n1));
end
```

Acknowledgements. This work was supported by grants from CNPq (grant 483226/2011-4), FAPESP (grants 2012/072812-2) and CAPES (grants 1236-83/2012). A. Ojeda González thanks the CAPES and CNPq (grant 141549/2010-6) for his PhD scholarship and CNPq (grant 150595/2013-1, 503790/2012-5) for his postdoctoral research support.

References

Baroni, M. P. M. A., Wit, A. D., and Rosa, R. R.: Detrended fluctuation analysis of numerical density and viscous fingering patterns, Europhys. Lett., 92, 64002, doi:10.1209/0295-5075/92/64002, 2010. 589

Bashan, A., Bartsch, R., Kantelhardt, J. W., and Havlin, S.: Comparison of detrending methods for fluctuation analysis, Physica A, 387, 5080–5090, doi:10.1016/j.physa.2008.04.023, 2008. 590

NPGD
1, 583–613, 2014

Bolzan, M. J. A., Ramos, F. M., Sá, L. D. A., Neto, C. R., and Rosa, R. R.: Analysis of fine-scale canopy turbulence within and above an Amazon forest using Tsallis' generalized thermo-statistics, J. Geophys. Res., 107, 8063, doi:10.1029/2001JD000378, 2002. 599

Buldyrev, S. V., Goldberger, A. L., Havlin, S., Mantegna, R. N., Matsa, M. E., Peng, C.-K., Simons, M., and Stanley, H. E.: Long-range correlation properties of coding and noncoding DNA sequences: genbank analysis, Phys. Rev. E, 51, 5084–5091, 1995. 590

Burlaga, L. F.: Magnetic clouds, in: Physics of the Inner Heliosphere, Vol. 2, edited by: Schwenn, R. and Marsch, E., Springer-Verlag, New York, 1–2, 1991. 585

Burlaga, L. F., Sittler, E., Mariani, F., and Schwenn, R.: Magnetic loop behind an interplanetary shock: Voyager, Helios and IMP 8 observations, J. Geophys. Res., 86, 6673–6684, 1981. 585

Calzadilla, M. A. and Lazo, B.: Sheffield Space Plasma Meeting (2001) multipoint measurements vs. theory, in: Inproceedings. ESA: Non-lineal time series analysis of Dst geomagnetic index, 24–26 April 2001, Sheffield, UK, edited by: Warmbein, B., ESA Publications Division, SP-492, 121–125, 2001. 585

Campos-Velho, H. F., Rosa, R. R., Ramos, F. M., Pielke, R. A., Degrazia, G. A., Neto, C. R., and Zanandrea, A.: Multifractal model for eddy diffusivity and counter-gradient term in atmospheric turbulence, Physica A, 295, 219–223, ISSN 0378-4371, 2001. 599

Cocconi, G., Greisen, K., Morrison, P., Gold, T., and Hayakawa, S.: The cosmic ray flare effect, Nuovo Cimento, 8, 161–168, 1958.

Dasso, S., Mandrini, C., Démoulin, P., Luoni, M., and Gulisano, A.: Large scale MHD properties of interplanetary magnetic clouds, Adv. Space Res., 35, 711–724, 2005. 584, 585, 590

Heneghan, C. and McDarby, G.: Establishing the relation between detrended fluctuation analysis and power spectral density analysis for stochastic processes, Phys. Rev. E, 62, 6103–6110, ISSN 1063-651X, 2000. 590

Hu, K., Ivanov, P. C., Chen, Z., Carpena, P., and Stanley, H. E.: Effect of trends on detrended fluctuation analysis, Phys. Rev. E, 64, 011114, doi:10.1103/PhysRevE.64.011114, 2001. 590

Hurst, H. E.: Long-term storage capacity of reservoirs, T. Am. Soc. Civ. Eng., 116, 770–808, 1951. 588

Hurst, H. E., Black, R. P., and Simaika, Y. M.: Long-Term Storage: an Experimental Study, Constable, London, 145 pp., 1965. 585, 588

Huttunen, K. E. J., Schwenn, R., Bothmer, V., and Koskinen, H. E. J.: Properties and geoeffectiveness of magnetic clouds in the rising, maximum and early declining phases of solar cycle

NPGD
1, 583–613, 2014

23, Ann. Geophys., 23, 625–641, 2005, http://www.ann-geophys.net/23/625/2005/. 591, 598, 608
Kantelhardt, J. W., Zschiegner, S. A., Koscielny-Bunde, E., Havlin, S., Bunde, A., and Stanley, H. E.: Multifractal detrended fluctuation analysis of nonstationary time series, Physica A, 316, 87–114, 2002. 590
Kay, S. and Marple, S. J.: Spectrum analysis – a modern perspective, Proceedings of the IEEE, 69, 1380–1419, doi:10.1109/PROC.1981.12184, 1981. 589
Klausner, V., Ojeda, G. A., Domingues, M. O., Mendes, O., and Papa, A. R. R.: Study of local regularities in solar wind data and ground magnetograms, J. Atmos. Sol.-Terr. Phy., 112, 10–19, doi:10.1016/j.jastp.2014.01.013, 2014. 585
Klein, L. W. and Burlaga, L. F.: Interplanetary magnetic clouds at 1 AU, J. Geophys. Res., 87, 613–624, 1982. 585
Lepping, R. P., Burlaga, L. F., and Jones, J. A.: Magnetic field structure of interplanetary magnetic clouds at 1 AU, J. Geophys. Res., 951, 11957–11965, 1990.
Lepping, R. P., Acuña, M. H., Burlaga, L. F., Farrell, W. M., Slavin, J. A., Schatten, K. H., Mariani, F., Ness, N. F., Neubauer, F. M., Whang, Y. C., Byrnes, J. B., Kennon, R. S., Panetta, P. V., Scheifele, J., and Worley, E. M.: The WIND magnetic field investigation, Space Sci. Rev., 71, 207–229, 1995.
Little, M., McSharry, P., Moroz, I., and Roberts, S.: Nonlinear, biophysically-informed speech pathology detection, in: ICASSP 2006 Proceedings. 2006 IEEE International Conference on Acoustics, Speech and Signal Processing, 14–19 May 2006, Toulouse, France, PP. II, doi:10.1109/ICASSP.2006.1660534, 2006. 589, 591
Malamud, B. D. and Turcotte, D. L.: Self-affine times series: I. Generation and analyses, Adv. Geophys., 40, 1–90, doi:10.1016/S0065-2687(08)60293-9, 1999. 587, 588, 589, 590, 591, 599, 600
Mandelbrot, B. B.: The Fractal Geometry of Nature, Times Books, 480 pp., 1983. 587
Mandelbrot, B. B. and Ness, J. W. V.: Fractional brownian motions, fractional noises and applications, SIAM Rev., 10, 422–437, ISSN 00361445, 1968. 588
Mandelbrot, B. B. and Wallis, J. R.: Some long-run properties of geophysical records, Water Resour. Res., 5, 321–340, 1969. 585
Mcsharry, P. E. and Malamud, B. D.: Quantifying self-similarity in cardiac inter-beat interval time series, in: Computers in Cardiology, 459–462, doi:10.1109/CIC.2005.1588136, 2005. 591

NPGD
1, 583–613, 2014

Mielniczuk, J. and Wojdyllo, P.: Estimation of Hurst exponent revisited, Comput. Stat. Data An., 51, 4510–4525, 2007.
Morrison, P.: Solar-connected variations of the cosmic rays, Phys. Rev., 95, 646, 1954.
Narock, T. W. and Lepping, R. P.: Anisotropy of magnetic field fluctuations in an average interplanetary magnetic cloud at 1 AU, J. Geophys. Res., 112, A06108, doi:10.1029/2006JA011987, 2007. 592
Ojeda, G. A., Calzadilla, M. A., Lazo, B., Alazo, K., and Savio, S.: Analysis of behavior of solar wind parameters under different IMF conditions using two nonlinear dynamics techniques, J. Atmos. Sol.-Terr. Phy., 67, 1859–1864, doi:10.1016/j.jastp.2004.12.014, 2005. 596
Ojeda, G., A., Mendes, O., Calzadilla, M. A., and Domingues, M. O.: Spatio-temporal entropy analysis of the magnetic field to help magnetic cloud characterization, J. Geophys. Res., 118, 5403–5414, 2013. 585, 590, 591, 592, 596
Ojeda, G., A., Mendes, O., Domingues, M. O., and Menconi, V. E.: Daubechies wavelet coefficients: a tool to study interplanetary magnetic fluctuations, Geofis. Int., 53, 101–115, 2014. 585, 591, 592, 596
Pelletier, J. D. and Turcotte, D. L.: Self-affine times series: 2. Applications and models, Adv. Geophys., 40, 91–166, 1999. 587
Peng, C.-K., Buldyrev, S. V., Havlin, S., Simons, M., Stanley, H. E., and Goldberger, A. L.: Mosaic organization of DNA nucleotides, Phys. Rev. E, 49, 1685–1689, 1994. 589
Percival, D. B. and Walden, A. T.: Spectral Analysis for Physical Applications: Multitaper and Conventional Univariate Techniques, Cambridge University Press, Cambridge, New York, NY, USA, 583 p., ISBN 052135532 0521435412, 1993. 593
Piddington, J. H.: Interplanetary magnetic field and its control of cosmic-ray variations, Phys. Rev., 112, 589–596, doi:10.1103/PhysRev.112.589, 1958.
Price, C. P. and Newman, D. E.: Using the R / S statistic to analyze AE data, J. Atmos. Sol.-Terr. Phy., 63, 1387–1397, 2001. 585
Priestley, M. B.: Spectral Analysis and Time Series, Academic Press, London, New York, 890 pp., 1981. 587, 593
Ramos, F. M., Bolzan, M. J. A., Sá, L. D. A., and Rosa, R. R.: Atmospheric turbulence within and above an Amazon forest, Physica D, 193, 278–291, doi:10.1016/j.physd.2004.01.026, 2004. 602

NPGD
1, 583–613, 2014

Rosa, R. R., Karlický, M., Veronese, T. B., Vijaykumar, N. L., Sawant, H. S., Borgazzi, A. I., Dantas, M. S., Barbosa, E. B. M., Sych, R. A., and Mendes, O.: Gradient pattern analysis of short solar radio bursts, Adv. Space Res., 42, 844–851, ISSN 0273-1177, 2008. 602

Ruzmaikin, A., Feynman, J., and Robinson, P.: Long-term persistence of solar activity, Sol. Phys., 149, 395–403, 1994. 585

Smith, C. W., L'Heureux, J., Ness, N. F., Acuña, M. H., Burlaga, L. F., and Scheifele, J.: The ACE magnetic fields experiment, Space Sci. Rev., 86, 613–632, 1998.

Tapiero, C. and Vallois, P.: Run length statistics and the Hurst exponent in random and birth-death random walks, Chaos Soliton. Fract., 7, 1333–1341, doi:10.1016/0960-0779(96)00032-X, 1996. 589

Turcotte, D. L.: Fractals and chaos in geology and geophysics, 2nd revised Edn., Cambridge University Press, New York, USA, ISBN 0521567335, 1997. 587

Vandas, M., Odstrcil, D., and Watari, S.: Three-dimensional MHD simulation of a loop-like magnetic cloud in the solar wind, J. Geophys. Res., 107, 1236, doi:10.1029/2001JA005068, 2002. 585

Vanouplines, P.: Rescaled range analysis and the fractal dimension of pi, University Library, Free University Brussels, Pleinlaan 2, 1050 Brussels, Belgium, 1995. 589

Veronese, T., Rosa, R., Bolzan, M., Fernandes, F. R., Sawant, H., and Karlicky, M.: Fluctuation analysis of solar radio bursts associated with geoeffective X-class flares, J. Atmos. Sol.-Terr. Phy., 73, 1311–1316, doi:10.1016/j.jastp.2010.09.030, 2011. 589, 590, 594, 596

Voss, R. F.: Random fractals: characterization and measurement, in: Scaling Phenomena in Disordered System, edited by: Pynn, R. and Skjeltorp, A., Springer US, 1–11, doi:10.1007/978-1-4757-1402-9_1, 1985a. 587

Voss, R. F.: Random fractal forgeries. In: Fundamental Algorithms for Computer Graphics, NATO ASI, F17, edited by: Earnshaw, R. A., Springer-Verlag, Berlin Heidelberg, 805–835, 1985b. 587

Voss, R. F.: Characterization and measurement of random fractals, Phys. Scripta, 13, 27–32, 1986. 587

Wei, H. L., Billings, S. A., and Balikhin, M.: Analysis of the geomagnetic activity of the D_{st} index and self-affine fractals using wavelet transforms, Nonlin. Processes Geophys., 11, 303–312, doi:10.5194/npg-11-303-2004, 2004. 585

Zheng, H., Song, W., and Wang, J.: Detrended fluctuation analysis of forest fires and related weather parameters, Physica A, 387, 2091–2099, ISSN 0378-4371, 2008. 590

NPGD
1, 583–613, 2014

Table 1. Solar wind data studied (from Huttunen et al., 2005).

No.	Year	Shock, UT	MC start, UT	MC stop, UT	Pos-MC, UT
01	1998	6 Jan, 13:19	7 Jan, 03:00	8 Jan, 09:00	10 Jan, 15:00
02		3 Feb, 13:09	4 Feb, 05:00	5 Feb, 14:00	6 Feb, 23:00
03		4 Mar, 11:03	4 Mar, 15:00	5 Mar, 21:00	7 Mar, 03:00
04		1 May, 21:11	2 May, 12:00	3 May, 17:00	4 May, 22:00
05		13 Jun, 18:25	14 Jun, 02:00	14 Jun, 24:00	15 Jun, 22:00
06		19 Aug, 05:30	20 Aug, 08:00	21 Aug, 18:00	23 Aug, 04:00
07		24 Sep, 23:15	25 Sep, 08:00	26 Sep, 12:00	27 Sep, 16:00
08		18 Oct, 19:00	19 Oct, 04:00	20 Oct, 06:00	21 Oct, 08:00
09		8 Nov, 04:20	8 Nov, 23:00	10 Nov, 01:00	12 Nov, 02:00
10		13 Nov, 00:53	13 Nov, 04:00	14 Nov, 06:00	15 Nov, 08:00
11	1999	18 Feb, 02:08	18 Feb, 14:00	19 Feb, 11:00	20 Feb, 08:00
12		16 Apr, 10:47	16 Apr, 20:00	17 Apr, 18:00	18 Apr, 16:00
13		8 Aug, 17:45	9 Aug, 10:00	10 Aug, 14:00	11 Aug, 18:00
14	2000	11 Feb, 23:23	12 Feb, 12:00	12 Feb, 24:00	13 Feb, 12:00
15		20 Feb, 20:57	21 Feb, 14:00	22 Feb, 12:00	23 Feb, 10:00
16		11 Jul, 11:22	11 Jul, 23:00	13 Jul, 02:00	14 Jul, 05:00
17		13 Jul, 09:11	13 Jul, 15:00	13 Jul, 24:00	14 Jul, 09:00
18		15 Jul, 14:18	15 Jul, 19:00	16 Jul, 12:00	17 Jul, 05:00
19		28 Jul, 05:53	28 Jul, 18:00	29 Jul, 10:00	30 Jul, 02:00
20		10 Aug, 04:07	10 Aug, 20:00	11 Aug, 08:00	11 Aug, 20:00
21		11 Aug, 18:19	12 Aug, 05:00	13 Aug, 02:00	13 Aug, 23:00
22		17 Sep, 17:00	17 Sep, 23:00	18 Sep, 14:00	19 Sep, 05:00
23		2 Oct, 23:58	3 Oct, 15:00	4 Oct, 14:00	5 Oct, 13:00
24		12 Oct, 21:36	13 Oct, 17:00	14 Oct, 13:00	15 Oct, 09:00
25		28 Oct, 09:01	28 Oct, 24:00	29 Oct, 23:00	30 Oct, 22:00
26		6 Nov, 09:08	6 Nov, 22:00	7 Nov, 15:00	8 Nov, 08:00
27	2001	19 Mar, 10:12	19 Mar, 22:00	21 Mar, 23:00	23 Mar, 24:00
28		27 Mar, 17:02	27 Mar, 22:00	28 Mar, 05:00	28 Mar, 12:00
29		11 Apr, 15:18	12 Apr, 10:00	13 Apr, 06:00	14 Apr, 02:00
30		21 Apr, 15:06	21 Apr, 23:00	22 Apr, 24:00	24 Apr, 01:00
31		28 Apr, 04:31	28 Apr, 24:00	29 Apr, 13:00	30 Apr, 02:00
32		27 May, 14:17	28 May, 11:00	29 May, 06:00	30 May, 01:00
33		31 Oct, 12:53	31 Oct, 22:00	2 Nov, 04:00	3 Nov, 10:00
34	2002	23 Mar, 10:53	24 Mar, 10:00	25 Mar, 12:00	26 Mar, 14:00
35		17 Apr, 10:20	17 Apr, 24:00	19 Apr, 01:00	20 Apr, 02:00
36		18 May, 19:44	19 May, 04:00	19 May, 22:00	20 May, 16:00
37		1 Aug, 23:10	2 Aug, 06:00	2 Aug, 22:00	3 Aug, 14:00
38		30 Sep, 07:55	30 Sep, 23:00	1 Oct, 15:00	2 Oct, 07:00
39	2003	20 Mar, 04:20	20 Mar, 13:00	20 Mar, 22:00	21 Mar, 07:00
40		17 Aug, 13:41	18 Aug, 06:00	19 Aug, 11:00	20 Aug, 16:00
41		20 Nov, 07:27	20 Nov, 11:00	21 Nov, 01:00	22 Nov, 15:00

NPGD
1, 583–613, 2014

Table 2. We calculate the persistence in the IMF components by four different method: β exponent of power spectrum, α exponent of DFA, Hurst of R / S analysis and Hausdorff *Ha* exponent of semivariogram respectively. The interval from 6 January 13:19 UT to 7 January 02:59 UT 1998 was classified as sheath. The intervals 7 January 03:00 UT to 8 January 09:00 UT and from 8 January 09:01 UT to 9 January 15:00 UT were classified as MC and solar wind after the MC respectively. Dates are shown in Table 1, event No. 1.

Event No. 1	α	β	*Hu*	*Ha*
B_x:				
Sheath	1.27	1.71	0.86	0.31
MC	1.41	1.60	0.89	0.31
Pos-MC	1.31	1.70	0.87	0.31
B_y:				
Sheath	1.34	1.68	0.87	0.27
MC	1.52	1.55	0.91	0.42
Pos-MC	1.37	1.65	0.88	0.31
B_z:				
Sheath	1.39	1.65	0.85	0.31
MC	1.45	1.75	0.90	0.36
Pos-MC	1.23	1.64	0.86	0.23
Mean Values:	$\langle\alpha_{(j)}\rangle \pm \sigma$	$\langle\beta_{(j)}\rangle \pm \sigma$	$\langle Hu_{(j)}\rangle \pm \sigma$	$\langle Ha_{(j)}\rangle \pm \sigma$
Sheath	1.33 ± 0.06	1.68 ± 0.03	0.86 ± 0.01	0.30 ± 0.02
MC	1.46 ± 0.06	1.64 ± 0.11	0.90 ± 0.01	0.37 ± 0.05
Pos-MC	1.30 ± 0.07	1.66 ± 0.04	0.87 ± 0.01	0.28 ± 0.05

NPGD
1, 583–613, 2014

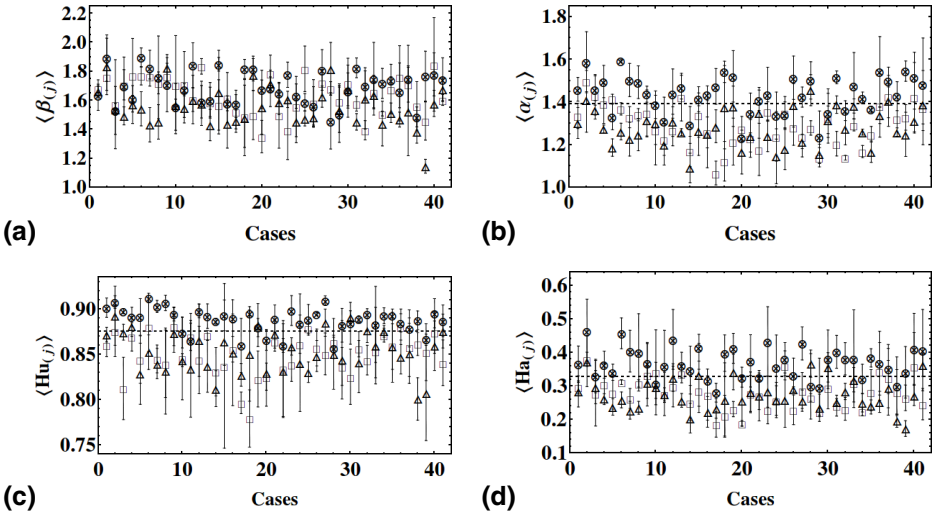

Fig. 1. In **(a)**, the PSD scaling exponent $\langle\beta_{(j)}\rangle$ values vs. number of events (see Table 1) were plotted, where ("□"), ("⊗") and ("Δ") symbols corresponds to the sheath, MC and post-MC regions respectively. The other panels **(b)**, **(c)** and **(d)** are similar to **(a)** but for $\langle\alpha_{(j)}\rangle$, $\langle Hu_{(j)}\rangle$ and $\langle Ha_{(j)}\rangle$ exponents respectively. The results in the four panels show long-range persistence in IMF time series ($1 < \langle\beta_{(j)}\rangle < 2$, $1 < \langle\alpha_{(j)}\rangle < 1.6$, $0.75 < \langle Hu_{(j)}\rangle < 0.95$ and $0.1 < \langle Ha\rangle < 0.5$). The horizontal dashed line is a threshold derived from Fig. 4.

NPGD
1, 583–613, 2014

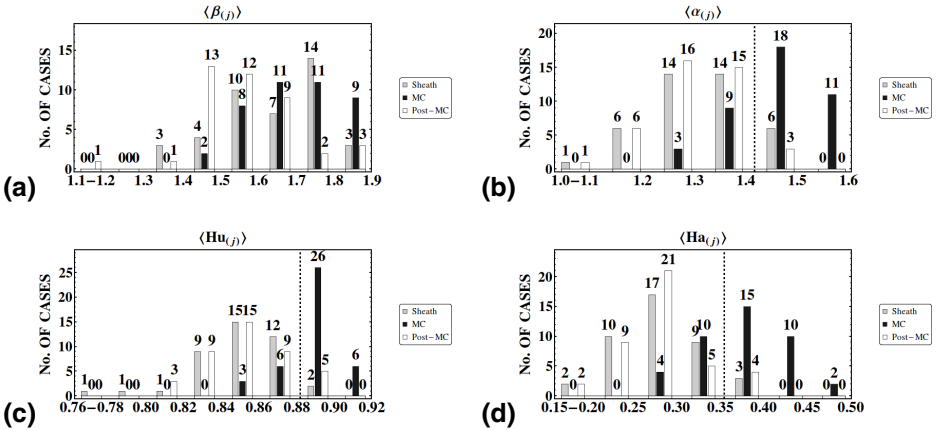

Fig. 2. In **(a)**, a histogram is construct from a frequency table of $\langle\beta_{(j)}\rangle$ values plotted in Fig. 1a. We want to have a better view of the distribution of $\langle\beta_{(j)}\rangle$ values between the three regions. The other panels **(b)**, **(c)** and **(d)** are similar to **(a)** but for $\langle\alpha_{(j)}\rangle$, $\langle Hu_{(j)}\rangle$ and $\langle Ha_{(j)}\rangle$ exponents respectively.

NPGD
1, 583–613, 2014

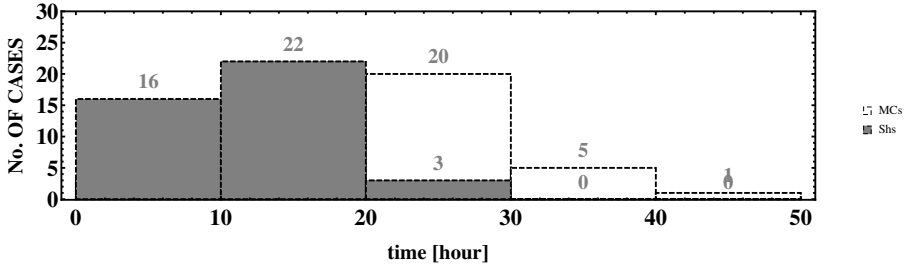

Fig. 3. Histogram from 41 MCs and its respective plasma sheaths that have been studied in this paper. The Histogram show the number of cases vs. temporal extension (in hour) of MCs and plasma sheaths respectively.

NPGD
1, 583–613, 2014

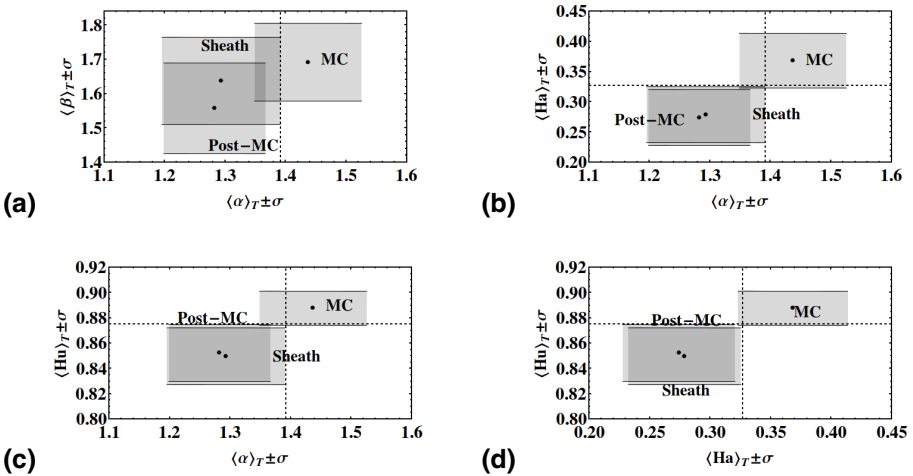

Fig. 4. In **(a)**, the black points are $(\langle\alpha_{(j)}\rangle_T, \langle\beta_{(j)}\rangle_T)$ in each of three regions, of the 41 events plotted in the Fig. 1a and b. We calculate the standard deviation of the mean for each persistence exponent that was shown in the Eq. (11). For 2-D graphic, filling is done in the x and y directions between the standard deviation of the mean. The filling rectangular regions are the set of validations of the persistence for each regions, $(\langle\beta_{(j)}\rangle_T \pm \sigma)$ vs. $(\langle\alpha_{(j)}\rangle_T \pm \sigma)$. The other panels **(b)**, **(c)** and **(d)** are similar to **(a)** but for other exponents combinations i.e.: **(b)** $(\langle Ha_{(j)}\rangle_T \pm \sigma)$ vs. $(\langle\alpha_{(j)}\rangle_T \pm \sigma)$; **(c)** $(\langle Hu_{(j)}\rangle_T \pm \sigma)$ vs. $(\langle\alpha_{(j)}\rangle_T \pm \sigma)$; **(d)** $(\langle Hu_{(j)}\rangle_T \pm \sigma)$ vs. $(\langle Ha_{(j)}\rangle_T \pm \sigma)$.

NPGD
1, 583–613, 2014